Synthesis, Solid-State, and Charge-Transport Properties of Conjugated Polythiophene-*S,S*-dioxides

Justin E. Cochran,[1] Elizabeth Amir,[2] Kulandaivelu Sivanandan,[2] Sung-Yu Ku,[2] Jung Hwa Seo,[2] Brian A. Collins,[3] John R. Tumbleston,[3] Michael F. Toney,[4] Harald Ade,[3] Craig J. Hawker,[1,2] Michael L. Chabinyc[2]

[1]Department of Chemistry and Biochemistry, University of California, Santa Barbara, California 93106-9510

[2]Materials Research Laboratory and Materials Department, University of California, Santa Barbara, California 93106-9510

[3]Department of Physics, North Carolina State University, North Carolina 27695

[4]Stanford Synchrotron Radiation Lightsource, SLAC National Accelerator Laboratory, Menlo Park, California 94025

Correspondence to: M. L. Chabinyc (E-mail: mchabinyc@engineering.ucsb.edu)

Received 20 June 2012; revised 9 August 2012; accepted 17 August 2012; published online
DOI: 10.1002/polb.23167

ABSTRACT: An alkylated semiconducting polymer comprising alternating bithiophene-[all]-*S,S*-dioxide and aromatic monothiophene units in the polymer backbone was synthesized with the intent of modifying the energy gap and lowest unoccupied molecular orbital for use as a stable *n*-type semiconductor. Films spun from this semiconducting polymer were characterized utilizing X-ray scattering, near edge X-ray absorption fine structure spectroscopy, ultraviolet photoelectron spectroscopy, and thin-film field effect transistors to determine how oxidation of the thiophene ring systems impacts the structural and electronic properties of the polymer. The thiophene-*S,S*-dioxide polymers have lower optical and electrical band gaps than corresponding thiophene polymers. X-ray scattering results indicate that the polymers are well ordered with the π–π stacking distances increased by 0.4 Å relative to analogous thiophene polymers. The electrical stability of these polymers is poor in transistors with a drop in the field effect mobility by approximately one order of magnitude upon addition of just 5% of the thiophene-*S,S*-dioxide unit in a copolymer with thiophene. © 2012 Wiley Periodicals, Inc. J Polym Sci Part B: Polym Phys 000: 000–000, 2012

KEYWORDS: polythiophene; polythiophene-*S,S*-dioxides; semiconducting polymers; thin film; X-ray scattering

INTRODUCTION Significant research efforts have been directed at the synthesis of new materials for organic-based electronics. The majority of semiconducting polymers exhibit *p*-type (hole-transporting) behavior.[1(a–d)] In contrast, organic semiconductors that exhibit air stable *n*-type (electron-transporting) and ambipolar conduction are far less developed.[2] Efficient complementary logic circuits require thin-film transistors (TFTs) with comparable electron and hole mobilities within the range of 1 $cm^2\ V^{-1}\ s^{-1}$ for relatively fast operation. Achieving this goal requires the development of stable, *n*-type organic semiconductors where the energy of the lowest unoccupied molecular orbital (LUMO) is lowered to allow efficient injection of electrons from air-stable metallic contacts, such as aluminum.

A number of *n*-channel and ambipolar semiconductors have been developed through synthetic design that lowers the LUMO for injection and stability. Although there are examples of homopolymers with *n*-type conduction,[3] the majority are copolymers with a donor–acceptor structure. For example, acceptors with low-lying LUMOs such as perylenedicarboximide,[4(a,b)] benzo[1,2-*c*;4,5-*c*′]bis[1,2,5]thiadiazole,[5] and indenofluorenebis (dicyanovinylene)[6] have been copolymerized with thiophene to achieve semiconducting polymers with high electron mobility. In these systems, it is beneficial to lower both the LUMO of the donor and the acceptor to achieve a substantially lowered LUMO in the combined donor–acceptor unit. A successful strategy to lower the LUMO of conjugated units, such as thiophene, has been incorporation of substituents with electron withdrawing groups, such as fluorine and/or carbonyl.[7(a–d)] Additional methodologies to control the LUMO of conjugated moieties will increase the range of accessible materials with *n*-type behavior.

A promising modification of thiophene to lower the energy of its LUMO involves oxidation of the thiophene sulfur atom to the corresponding *S,S*-dioxide.[8] This oxidation causes the thiophene ring to lose aromaticity while inserting a strong electron-withdrawing group into the π-conjugated main chain.[9(a–e)] Although stable monothiophene-*S,S*-dioxides were described long ago,[10(a–c)] their fully oxygenated oligomers remained unknown because of the lack of synthetic

Additional Supporting Information may be found in the online version of this article.

methodology to produce them. Recently, access to oligothiophene-[all]-*S*,*S*-dioxides became possible with the introduction of a strong oxidizing reagent, $HOF{\cdot}CH_3CN$, which allows complete oxygenation of aromatic oligothiophenes.[11] Significant reductions in both energy gap (E_g) and LUMO levels were reported for the oligothiophene-[all]-*S*,*S*-dioxides in comparison with their aromatic precursors.

Here, we report morphological and electrical characterization in TFTs of an alkylated semiconducting polymer containing alternating bithiophene-[all]-*S*,*S*-dioxide and aromatic monothiophene units in the polymer backbone (**1**).[12] In this polymer, the incorporation of the highly electron-deficient bithiophene-[all]-*S*,*S*-dioxide unit lowers the LUMO energy, enhances polymer rigidity, and π-conjugation, affording a low-band gap material. Polymer **1** had good molecular ordering as measured by wide angle X-ray scattering and the molecular ordering in the polymer appears similar to that observed in oligomers. The field-effect mobility of carriers and their stability in **1** was studied in comparison with its aromatic analogue **2**. Despite the promising reduction in the LUMO in **1**, the introduction of *S*,*S*-dioxide resulted in a decrease to a complete loss in the electrical properties of TFTs depending on the degree of incorporation of the unit.

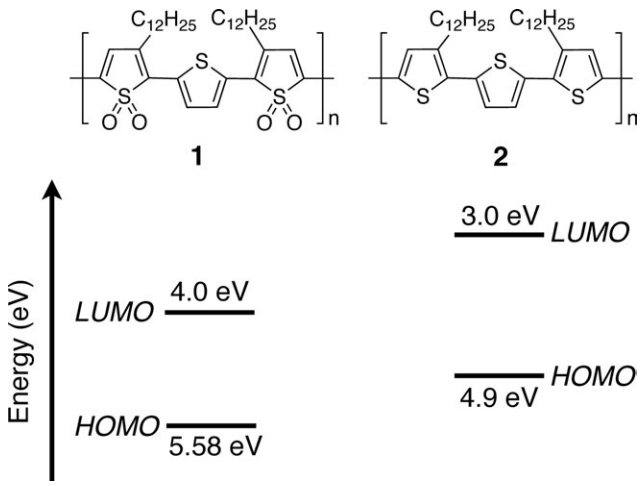

FIGURE 1 Energies of the HOMO for the as-cast polymers **1** and **2** determined from UPS measurements. The energies of the LUMOs were estimated by addition of the optical gap.

EXPERIMENTAL

Material Synthesis

Chemical structures of the polymers **1** and **2** are shown in Figure 1. The synthetic route to polymer **1** can be found in ref. 12 and a brief description can be found in the Supporting Information. Polymer **2** was obtained by removing the oxidation step from the synthesis of **1**. Polymer **1** and polymer **2** were soluble in chloroform or chlorobenzene and had $M_n = 10$ K (polydispersity [PDI] = 1.9) and $M_n = 11$ K (PDI = 1.5), respectively. As discussed previously, the molecular weight of **1** is relatively low owing to the lower reactivity of the bithiophene-[all]-*S*,*S*-dioxide comonomer.[12] The molecular weight of the thiophene analog, **2**, was synthesized to match that of **1** to isolate the electronic effects on transport rather than the effects of molecular weight.

Fabrication of Thin Films

Solutions consisting of 10–20 mg/mL of polymers **1** and **2** were mixed with a teflon stir bar in anhydrous chlorobenzene or a mixture of 1:1 anhydrous chlorobenzene: orthodichlorobenzene. Antimony-doped silicon consisting of a native oxide, 1–2 nm, or 150 nm thermal oxide was used as substrate. Substrates were cleaved to sizes ranging from 1 × 1 cm to 2.5 × 2.5 cm and then cleaned in piranha acid followed by sonication in acetone and isopropanol for 20 min each and finally plasma cleaned for 2 min just before use. A monolayer of *n*-octadecyltrichlorosilane (OTS) was solution deposited from a mixture of OTS and *n*-hexadecane.[13] Substrates were then rinsed with hexane, acetone, isopropanol, and dried with nitrogen gas. Polymer solutions were spin cast onto clean bare substrates, OTS-modified substrates, and substrates with 90 nm of thermally evaporated gold at speeds between 800 and 1400 rpm to form films between 60 and 100 nm thick. Films were either stored as-cast or annealed in a nitrogen-filled glovebox for 10 min at varying temperatures, between 110 and150 °C, to remove residual solvent and promote crystallization.

X-ray Scattering

Samples on silicon substrates with a native oxide layer were measured at the Stanford Synchrotron Radiation Lightsource. A grazing incidence wide-angle X-ray scattering (GIWAXS) geometry was used for beamline 11-3 with a MAR345 image detector, whereas a point detector was used for specular diffraction on beamline 2-1. GIWAXS beamline 11-3 was set at an energy of 12.7 keV, corresponding to a wavelength of 0.97 Å, and specular beamline 2-1 was set at an energy of 8 keV. Two pairs of soller slits defined the diffracted beam resolution as 0.002 Å. GIWAXS samples were annealed *in situ* for direct comparison between annealed films under a nitrogen atmosphere, whereas specular samples were different films/substrates due to time limitations resulting in a 5- to 8-nm thickness variation. All X-ray-characterized films were kept to within a ±15-nm thickness variation to avoid issues with thickness dependence. All X-ray samples were measured under a helium environment to minimize beam damage. Under GIWAXS conditions, the films were illuminated at an incident angle of 0.12° so that the beam penetrates the entire polymer film and only a portion of the silicon substrate.[14] Data are expressed in terms of the scattering vector, $\boldsymbol{q}$, with a magnitude equal to $(4\pi/\lambda)\sin\theta$, where θ is one half the scattering angle and λ is the wavelength of the incident radiation. The peak *d*-spacing was calculated by setting it equal to $2\pi/\boldsymbol{q}$. GIWAXS data were analyzed using WxDiff[15] and an analysis routine in Igor Pro (courtesy of R. J. Kline, NIST).

Near Edge X-ray Absorption Fine Structure Spectroscopy

NEXAFS spectra were acquired in transmission mode at the 5.3.2.2 beamline of the Advanced Light Source. A scanning transmission X-ray microscope rastered the beam across the film and through a hole in the film for each energy to record

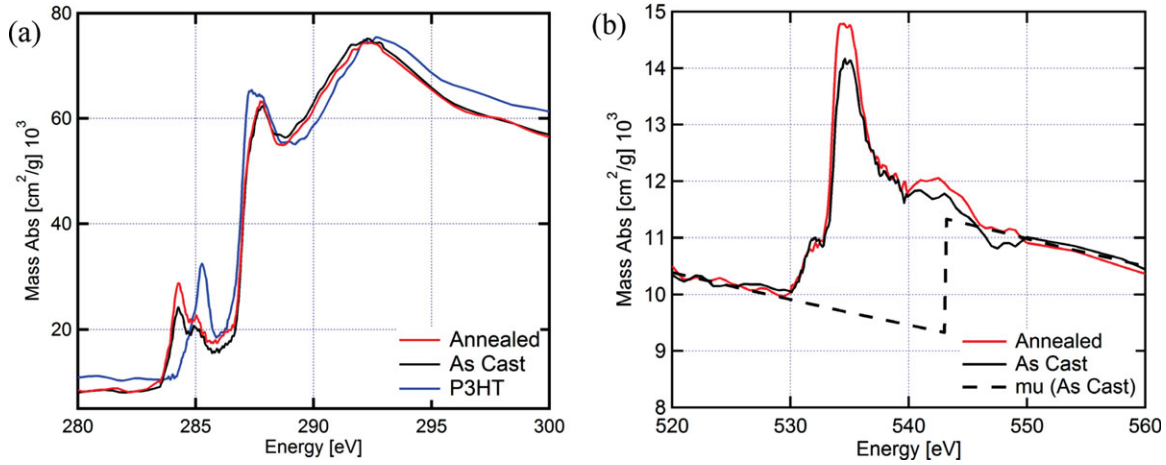

FIGURE 2 NEXAFS spectra measured at the (a) carbon edge for the reference P3HT film, blue line, and the as-cast, black line, and annealed, red line, film of **1** as well as at the (b) oxygen edge for the as-cast, black line, and annealed, red line, film of **1**.

the incident and transmitted beam simultaneously with the same detector. The energy was calibrated with a partial pressure of CO_2, noting the carbon and oxygen Rydberg states. The acquired spectra were then normalized above the edge (~380 eV) for carbon and below the edge (~520 eV) for oxygen to the bare atom mass absorption of a monomer. Polymer **1** was spin cast onto silicon substrates with 150 nm of thermal oxide. Films were annealed under nitrogen at 110 °C for 10 min and then initially floated in a 5% solution of hydrofluoric acid to etch off part of the thermal oxide. The final set of as-cast and annealed films were floated in deionized water and picked up on copper transmission electron microscopy (TEM) grids for spectral measurements. For comparison, NEXAFS of poly(3-hexylthiophene) (P3HT) films were also acquired, were spun cast from chlorobenzene solutions onto sodium polystyrene sulfonate-coated Si wafers. The films were annealed at 150 °C for 30 min to improve crystallinty. The P3HT film was floated in deionized water and picked up in copper TEM grids for spectral measurements.

Infrared spectroscopy

Fourier transform infrared (FTIR) spectroscopy was performed on thin films of **1** and **2** using a Perkin Elmer Spectrum 100 FTIR spectrometer. Films were spun on silicon substrates and processed in the same manner as X-ray and transistor samples.

Fabrication of TFTs

Bottom gate TFTs were made on thermal SiO_2/Si wafers where the gate contact was made by scratching through the oxide layer and utilizing silver paint to form contact with the probe station chuck. Source and drain contacts of either gold or aluminum were evaporated through a shadow mask onto the semiconducting film to a thickness of 90 nm. TFTs were measured under ambient, nitrogen, and vacuum using a Lakeshore TTP5 probe station and 2 Kiethley 2400 SMU run under a Lab View routine. The parameters of the TFTs, including mobility and threshold voltage, were extracted from the transfer curves.[16]

RESULTS AND DISCUSSION

Electronic Structure

The electronic structure of the *S,S*-dioxide polymer **1** shows significant differences from the thiophene analog **2** as reported previously.[12] The optical bandgap of **1** with the bithiophene-[all]-*S,S*-dioxide unit was 1.55 eV, estimated by the onset point of the absorption band, is significantly lower than the optical bandgap of polymer **2** (1.85 eV) and *rr*-P3HT (1.9 eV). The energies of the HOMO levels determined by ultraviolet photoelectron spectroscopy (UPS) for as-cast films of polymers **1** and **2** are −5.58 and −4.90 eV, respectively (Fig. 1 and Supporting Information Material). The energies of the LUMOs were estimated by adding the optical gap to the energy of the HOMO level; the uncertainty in the energy of the LUMO is the unknown value of the exciton binding energy, typically ~0.4 eV.[17] The LUMO energy of the aromatic polymer **2** is −3.05 eV, whereas the LUMO of polymer **1** is lower by about 1 eV (−4.03 eV). UPS measurements also revealed that annealing at 110 °C for 5 min lowered the HOMO energies in both polymers to a value of −5.77 eV for **1** and −4.97 eV for **2**.

To further explore the electronic structure of the two polymers and their ordering in thin films, we obtained NEXAFS spectra of the polymers at the carbon and oxygen edges. Carbon NEXAFS spectra of annealed and as-cast films of **1** are shown along with that of P3HT for comparison (Fig. 2). There are two π^* resonances for **1** at 284.3 and 285.0 eV, both of which are lower in energy than that of the single resonance of P3HT at 285.3 eV. The lower energy of the resonance is consistent with a lowered LUMO level relative to P3HT and the estimates from UPS spectra. Interestingly, the two features for **1** are similar to those reported for cis and trans polyacetylene.[18] This observation in combination with the shift in electronic levels suggests that the thiophene-*S,S*-dioxide ring more resembles a conjugated diene than a

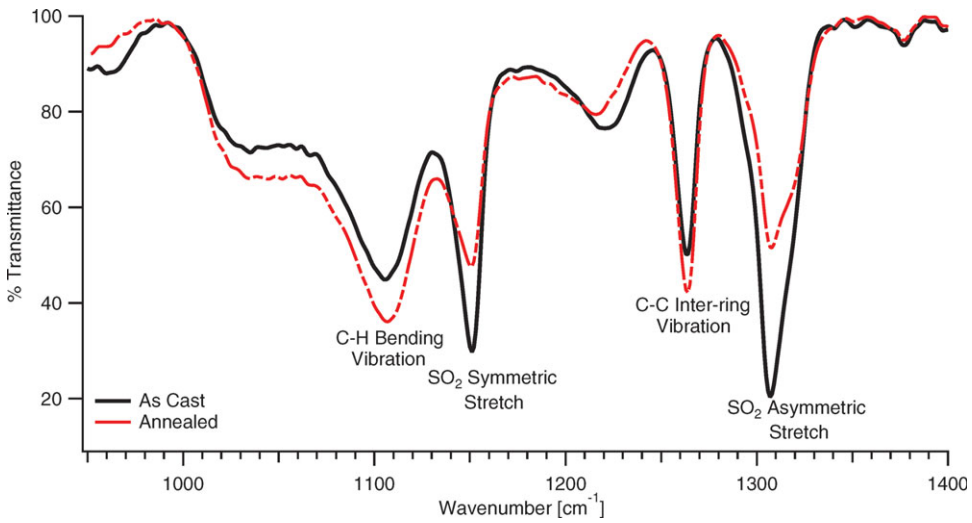

FIGURE 3 FTIR spectra of thin films of **1** in the region 950–1400 cm^{-1} The as-cast film is the solid black line, whereas the red dashed line is a film annealed at 150 °C. The labeled peaks are SO_2 stretches at 1150 and 1310 cm^{-1}, C—H bending at 1105 cm^{-1}, and C—C inter-ring stretches at 1264 cm^{-1}.

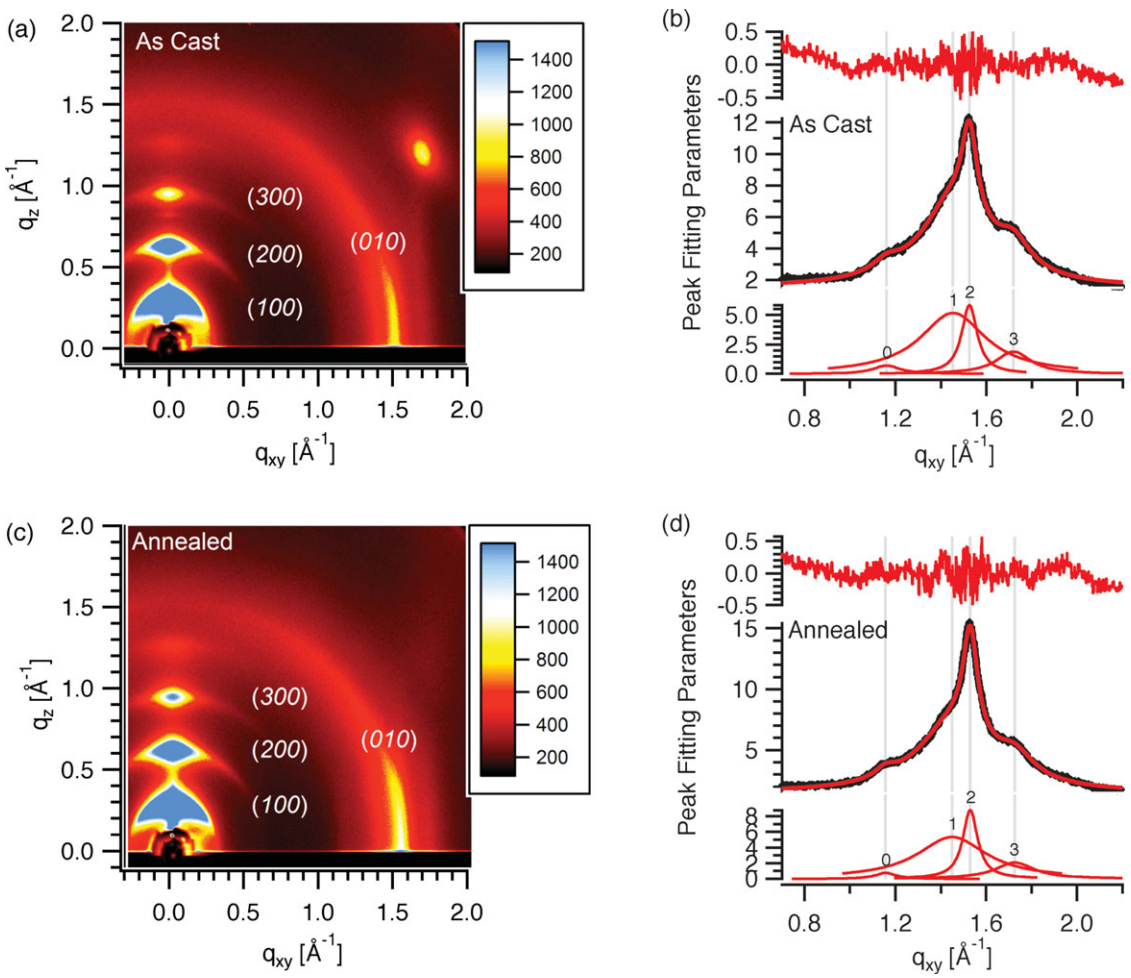

FIGURE 4 GIWAXS scattering pattern for (a) as-cast and (c) annealed films of polymer 1. Scattering data along q_{xy} (black line) and model peaks (red) are given for the (b) as-cast and (d) annealed films. The proposed crystallographic indices are listed in Table 2.

TABLE 1 Observed *d*-Spacings, FWHM, and Crystallite Thickness (t_{WH}) from High-Resolution Specular Scattering and GIWAXS for Polymers 1 and 2

	Specular Scattering				
Polymer film	(*100*) (Å)	FWHM (Å^{-1})	(*200*) (Å)	FWHM (Å^{-1})	t_{WH} (*h00*) (Å)
1 As–cast	19.92	0.047	10.08	0.063	148.7
1 Annealed 110 °C	19.88	0.065	9.84	0.060	111.2
1 Annealed 150 °C	19.67	0.055	9.76	0.063	152.9
2 As–cast	19.57	0.034	9.73	0.045	207.9
2 Annealed 150 °C	19.63	0.020	9.78	0.027	365.2

	GIWAXS				
Polymer film	(*100*) (Å)	FWHM (Å^{-1})	(*010*) (Å)	FWHM (Å^{-1})	t_{WH} (*h00*) (Å)
1 As–cast	20.33	0.048	4.1	0.08	335.1
1 Annealed 110 °C	20.63	0.050	4.1	0.08	306.6

thiophene ring.[19] Electronic structure calculations also show that the LUMO orbital has little contribution from the *S,S*-dioxide group in agreement with this interpretation (Supporting Information Material). Annealing of the films results in a small increase of the π^* resonance intensities in the spectra, which could be attributed to changes in chemical bonding or a change in molecular orientation relative to the substrate.[20]

NEXAFS spectra taken at the oxygen edge provided more insight into the spectral changes with thermal annealing. The overall height of the edge is not affected by annealing, showing that very little oxygen if any has been lost, while the σ^* resonance at 534.6 eV is significantly enhanced upon annealing. This change suggests that the nature of bonding between the oxygen and the sulfur has changed in character to resemble that of an ether rather than a sulfonic acid and demonstrates that a change in the bonding state in the molecule, rather than loss of oxygen, is a predominant effect of thermal annealing.[21] These data suggest that the shift in the HOMO upon annealing in **1** is also due to the change in bonding in the thiophene-*S,S*-dioxide unit.

Chemical Degradation

IR spectroscopy was performed on thin films of **1** and **2** to determine if chemical degradation of the oxygenated thiophene units occurred during thermal annealing. Sulfur–oxygen vibrational modes are typically found between 1000 and 1420 cm^{-1}. The results for as-cast films of **2** and one annealed at 150 °C showed no indication of symmetric or asymmetric SO_2 stretches, indicating that there is no observed oxidation of the thiophene ring as expected (Supporting Information Fig. S2). For polymer **1**, both symmetric, 1150 cm^{-1}, and asymmetric, 1307 cm^{-1}, SO_2 stretches are observed in the as-cast and annealed films (Fig. 3).[22(a,b)] The intensity of these peaks decreases upon annealing and can be seen by the change in ratio of the SO_2 stretches to nearby C—C inter-ring stretching modes at 1264 cm^{-1} and C—H bending mode at 1105 cm^{-1}.[23] These data support the interpretation of the changes in the NEXAFS spectra and provide evidence that a chemical change in the backbone occurs upon heating. This change in chemical composition also rationalizes the changes in structural ordering from X-ray scattering (*vide infra*).

Structural Ordering

Wide-angle X-ray scattering (WAXS) from films of **1** and **2** was measured to assess the structural changes caused by incorporation of thiophene-*S,S*-dioxide into the conjugated backbone. WAXS was measured for the polymers both at specular and at grazing incidence (GIWAXS). Similar to other conjugated polymers, the specular scattering from as-cast films of **1** and **2** revealed a progression of first and higher order peaks with the fundamental (*100*) *d*-spacing of 19.9 and 19.57 Å respectively (Fig. 4 and Table 1). In the GIWAXS,

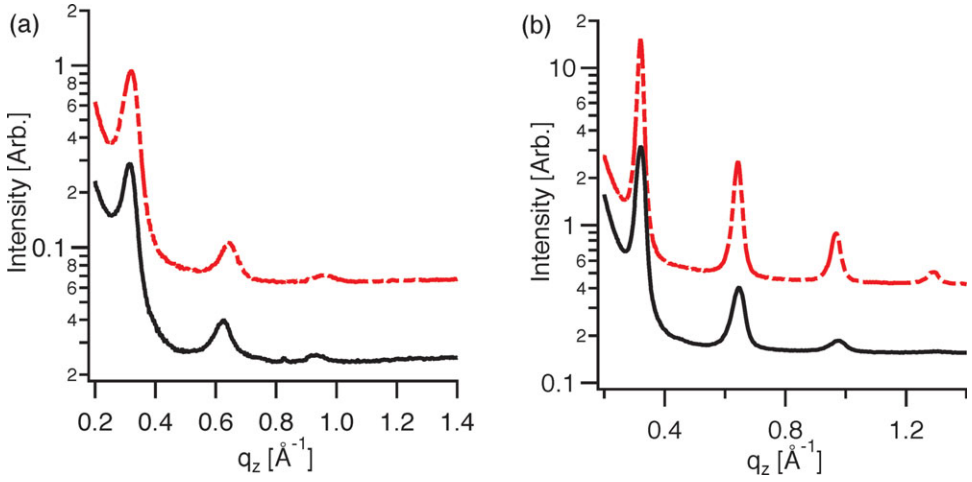

FIGURE 5 Specular X-ray scattering of the as-cast (black lines) and annealed (red dashed lines) films of (a) polymer **1** and (b) polymer **2**.

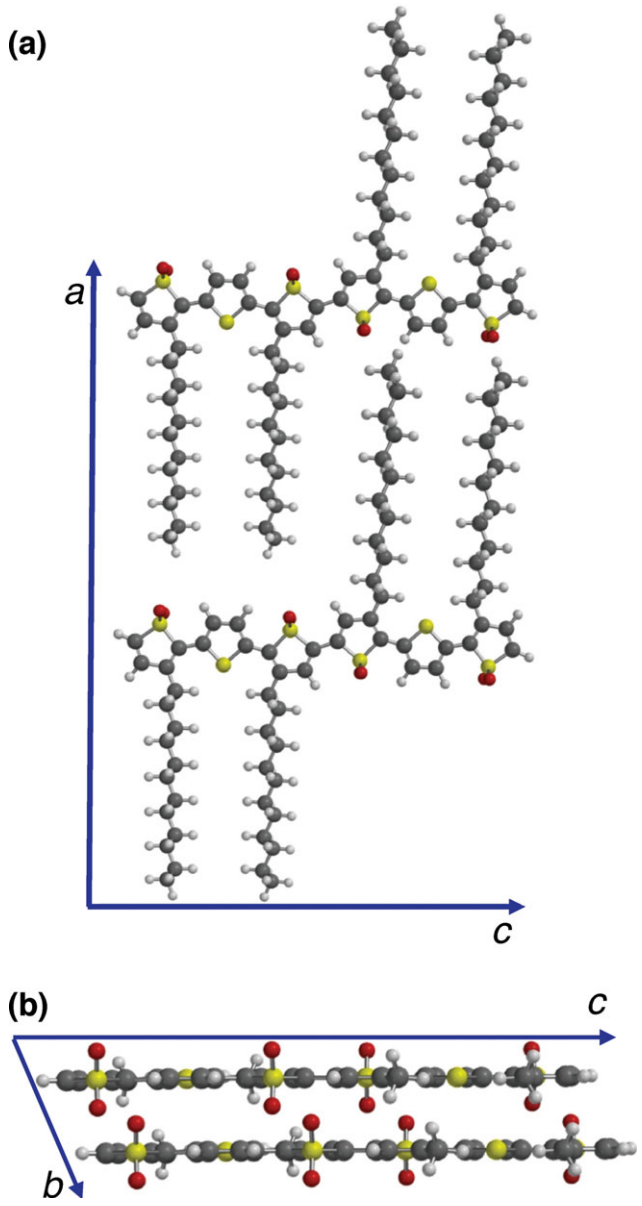

FIGURE 6 Theoretical packing model showing the repeat unit with respect to the *a*,*b*, and *c*-axis. The slip-stacking packing motif is shown (b) by following the shift in the red oxygen atoms.

four peaks along q_z assigned as (*100*) through (*400*) are observed for polymer **1**, whereas only three peaks are observed in the specular scan (Fig. 5). This difference may be a result of beam damage in the specular scans; the (*400*) peak is measured under the longest exposure time at the end of the acquisition. A small peak at a q_z of 0.82 $Å^{-1}$ can be observed in the as-cast films of polymer **1** in both the GIWAXS and the specular scans but disappears upon annealing. A diffuse scattering region in the GIWAXS image is visible near a q_z of 1.5 $Å^{-1}$ that is, in part, due to the amorphous halo and possibly the associated (*010*) band (Fig. 4).[24] For polymer **1** under both processing conditions, peaks are observed along q_{xy} at *d*-spacings of 3.68, 4.14, 4.38, and 5.47 Å; fit parameters can be found in the Supporting Information data and Figure 4.

To develop a structural model for the molecular packing of **1**, we first consider a structurally similar poly(thiophene). The backbone structures of polymers **1** and **2** are similar to that of poly(3,3′-dihexylterthiophene), P33DHTT, reported by Gallazzi et. al.[25] They proposed that the side chains of P33DHTT interdigitate, resulting in a smaller interchain spacing than for noninterdigitated sidechains.[20] The *d*-spacing values reported for P33DHTT were 13.03 Å for the separation of the backbones by the side chains (lamellar spacing) and 3.76 Å for the π–π stacking spacing.[20,26]

The lateral interactions of the π-stacked backbones in **1** were expected to differ from poly(dialkylterthiophenes) owing to addition of the thiophene-*S,S*-dioxide unit. Most reported values for π-stacking distance of poly(alkylthiophenes) chains are 3.8 $\pm$ 0.04 Å; therefore, any significant change outside of this range is likely caused by the presence of the oxygenated thiophene unit. There is also the possibility that the electron-rich oxygen units will repel nearby thiophene-*S,S*-dioxide units causing the adjacent chains of **1** to shift relative to each other. This shift would be similar to the stacking interactions observed in single crystal structures of oligomers of thiophene-*S,S*-dioxide.[11] This motif is referred to as slip-stacked packing and has been observed in substituted acenes depending on substituent size and position.[27] The slip-stacked packing motif allows for smaller π–π stacking distances at the cost of π-overlap between adjacent aromatic units.

Our WAXS data support a structural model for **1** where the side chains are interdigitated and that adjacent chains are slip-stacked relative to each other. The *n*-dodecyl side chains of **1** and **2** are longer than the *n*-hexyl chains in P33DHTT and are expected to cause an increase in the (*h00*), interlayer *d*-spacing of ~1.25 Å/methylene, which is close to the observed spacing difference.[28] The result of alkyl chain interdigitation is that the oxygenated thiophene units on each monomer unit are forced to be in a *syn* configuration; the resulting chain-to-chain backbone interactions lead to slipping along the adjacent backbone to accommodate electronic and steric interactions. The geometry of the repeat units was calculated using molecular orbital theory at the HF/6-31G* level of theory, which is known to produce reasonable bond

TABLE 2 Predicted and Observed Peak Positions for In-Plane Scattering Peaks of Polymer 1[a]

Peak Assignment [*hkl*]	Predicted *d*-Spacing (Å)	Observed *d*-Spacing (Å)
[*010*] (2)	4.14	4.1
[*004*] (0)	5.48	5.5
[*005*] (1)	4.39	4.4
[*006*] (3)	3.66	3.7

[a] The numbers in parenthesis next to the peak assignment correlate to the peaks labeled in Figure 4.

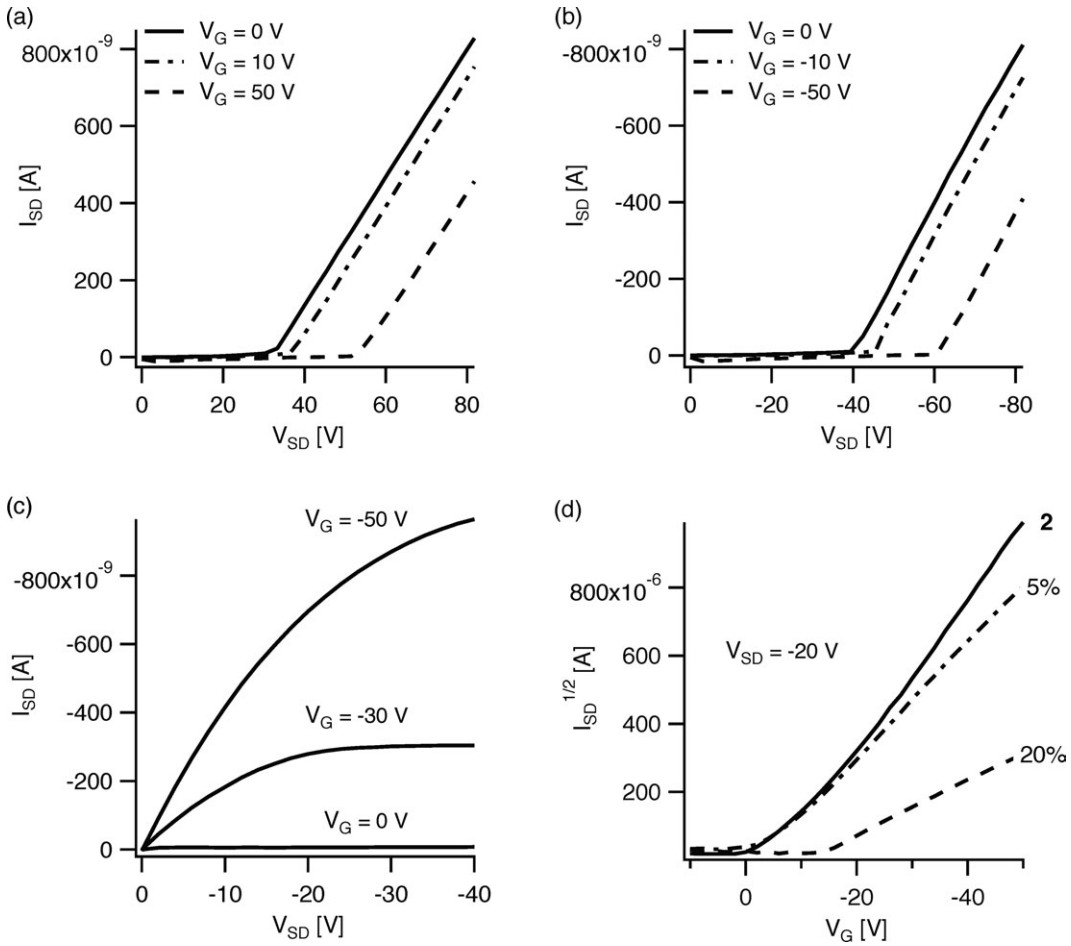

FIGURE 7 Device characteristics of TFTs for each of the polymers. (a) *n*-Type and (b) *p*-type output characteristics of polymer **1** (c) *p*-type output characteristics of polymer **2** at a V_G of 0, −30, and −50 V. (d) Transfer characteristics at $V_{SD} = -20$ V for polymer **2**, 5% incorporation of thiophene-*S,S*-dioxide, and 20% incorporation of thiophene-*S,S*-dioxide.

lengths and angles for ground-state organic molecules.[29] A model monoclinic unit cell with $\beta = 69°$ and a *c*-axis length equals to that of two monomer units has a predicted (*010*) *d*-spacing of 4.14 Å as shown in Figure 6. This model enabled the assignment of the additional in-plane peaks (Table 2). Although we have made an assignment of the unit cell, we have not attempted to model the exact placement of the polymer chains in the cell and therefore do not know whether the chains are tilted with respect to one another as observed for other thiophene copolymers.[30] Despite this uncertainty, it is still clear that the backbones in **1** are farther away from each other than typical semicrystalline poly(alkylthiophenes). This increase in "π–π" spacing has a potential adverse effect on transport because of the decrease in π-overlap reducing the intermolecular coupling.[31] An increase in "π–π" spacing coupled with a decrease in π-overlap, due to the slip of the backbone, could cause a decrease in the measured field effect mobility of **1** when compared to the aromatic analogue **2**.

The change from thiophene to thiophene-*S,S*-dioxide also affects the microstructure of the films. Comparison of the as-cast films of polymer **1** and **2** indicates that addition of the SO_2 unit causes an increase in the full width at half maximum (FWHM) of the (*100*) of **1** correlating to a decrease in crystallite size, 20.8 nm (**2**) compared to 14.9 nm (**1**), as calculated by the Williamson–Hall method (Supporting Information). A similar scattering pattern is observed in the polymer **1** GIWAXS annealed *in situ* and as-cast samples. The in-plane scattering, q_{xy}, peaks show an increase in intensity upon annealing but no change in peak position or width. No new peaks were observed in the GIWAXS pattern after the *in situ* annealing. The spread of the scattering intensity with respect to the polar angle provides information about the distribution of orientation of crystalline grains in a polycrystalline-film; the spread of the (*h00*) peaks of 1 increases with annealing indicating an increase in the range of orientations. This is shown in Figure 4 by comparing the arching of the (*200*) peaks for the two film conditions of **1**. These observations are attributed to an increase in the number of crystallites misoriented relative to the surface normal and are consistent with the decrease in size of crystallite.[32] These results are different to those observed for **2** (Table 1) and other thiophene-based systems where an increase in intensity and a decrease in peak width is observed upon

annealing.[22,33] The change in bonding observed in the NEXAFS and FTIR spectra upon annealing suggests that at least part of the disorder induced by thermal annealing results from chemical changes. Based on these observations, one can conclude that the oxygenated thiophene unit has an adverse affect on film order, causing a decrease in crystallite size and increase in disorder in films of **1**.

Electrical Performance

The electrical performance of both **1** and **2** was investigated using TFTs fabricated with contacts to probe hole and electron injection. The energy levels as measured by UPS indicate that holes can readily be injected from Au contacts into both **1** and **2**, but electrons could also be injected from Al contacts for **2**. The current–voltage (*I*–*V*) data for TFTs made with polymer **2** had "ideal" behavior as *p*-type TFTs and good stability, similar to other thiophene devices (Fig. 7).[16] The as-cast saturation hole mobility was $2.3 \pm 0.4 \times 10^{-3}$ $cm^2\ V^{-1}\ s^{-1}$, comparable to P3HT of similar molecular weight, geometry, and processing but lower than values published for poly(3,3′-dioctylterthiophene).[20,21] Although *I*–*V* measurements of TFTs of polymer **1** suggested the possibility of ambipolar behavior, the TFTs had relatively low absolute currents, on the order of 10^{-9} A and never exhibited single-carrier transport characteristics even at high gate voltages, $>\pm 80$ V, in either hole or electron accumulation regimes (Fig. 7). Although OTS-modified SiO_2 can be a poor dielectric for ambipolar material due to tunneling and potential charge trapping by silanol groups,[2] TFTs should operate for a short period before the charge traps fill. Even pulsed gate measurements, pulse width on the order of 100 μs, did not reveal stable gated conduction with contacts formed from either gold or aluminum. It was also observed that the low current observed in TFTs with gold contacts was dependent on the history of operation including the direction of voltage sweep and the sign of the applied bias.

As both **1** and **2** had similar molecular weight and similar morphology, we hypothesized that the difference in performance of TFTs is because of the instability of the *S*,*S*-dioxide unit. Although the films of **1** used in TFTs were not thermally annealed, it is likely that the formation of charge carriers could also impact the labile SO_2 functionality. To test this possibility, we examined a series of random copolymers with a lower density of thiophene-*S*,*S*-dioxide units, 5% (95% S:5% SO_2) and 20% (80% S:20% SO_2) by monomer. These polymers exhibited similar structural ordering to **1** and **2** (Supporting Information Fig. S6). For direct comparison to polymer **2**, the same geometry, dielectric, and processing conditions were used. TFTs with these polymers exhibited saturation hole mobilities of $1.9 \pm 0.6 \times 10^{-3}$ $cm^2\ V^{-1}\ s^{-1}$ (5%) and $8.5 \pm 0.3 \times 10^{-4}$ $cm^2\ V^{-1}\ s^{-1}$ (20%) (Fig. 7). Higher incorporation of the oxygenated thiophene unit resulted in a threshold voltage shift as well as a decrease in mobility. Upon thermal annealing at 110 °C (where we expect degradation of the SO_2 group based on FTIR data), both devices exhibited lower currents with complete failure observed with $\geq$20% incorporation. These results suggest that despite the ability to control the HOMO and LUMO levels, the *S*,*S*-dioxide unit has an adverse impact on electrical operation at the high carrier densities in TFTs. The charge carrier mobility in semiconducting polymers is highly sensitive to impurities that are difficult to detect with bulk analytical methods, for example 1 part per million of contaminant can have a detrimental impact on conduction if the contaminant forms an electrically active species.[34(a,b)] Degradation of the dioxygenated thiophene would likely result in a break in the conjugation of the backbone or a disruption in the π-stacking, all of which can decrease the carrier mobility.

CONCLUSIONS

We have synthesized and characterized a series of polymers and copolymers based on thiophene and thiophene-*S*,*S*-dioxide. X-ray scattering shows that the thiophene-*S*,*S*-dioxide polymer **1** forms semicrystalline, textured films with a similar structure to poly(3,3′-dialkyterthiophenes). Incorporation of the oxygenated thiophene units in the backbone leads to films that are still semicrystalline, but with smaller estimated crystallite sizes. An increase in the in-plane *d*-spacing compared to the structurally similar terthiophene polymer **2**. Upon thermal annealing, polymer **1** undergoes a decrease in crystallite size, but does not undergo changes in texture. NEXAFS and FTIR data suggest that the *S*,*S*-dioxide units undergo a change in bonding during thermal treatment.

Based on the electrical data from TFTs with polymers with varying ratio of thiophene-*S*,*S*-dioxide to thiophene, it is clear that incorporation of small amounts of oxygenated thiophene in the polymer backbone has a minimal impact on overall device performance, resulting in a slight performance decrease and stability. It appears that increasing the number of oxygenated thiophene units above 5% by monomer in the backbone results in significant degradation, limiting the ability of charge carriers to traverse the film. It is important to note that although polymer **1** is relatively crystalline it does not directly indicate good electronic properties.[34] The incorporation of a significant quantity of thiophene-*S*,*S*-dioxide into the backbone leads to a more pronounced "slip-stacking" effect changing the electronic coupling between chains. In addition, the degradation products of the oxygenated thiophene units may be acting as localized long lifetime trap sites thereby decreasing the carrier mobility of both holes and electrons.

ACKNOWLEDGMENTS

M. L. Chabinyc and J. E. Cochran are supported by NSF (DMR-0906224) and B. A. Collins, J. R. Tumbleston and H. Ade supported by NSF (DMR-0906457) both of which were funded under the American Recovery and Reinvestment Act. Analytical work was carried out using the MRL Central Facilities supported by the MRSEC Program of the NSF under Award No. DMR 1121053; a member of the NSF-funded Materials Research Facilities Network (www.mrfn.org). Portions of this research were carried out at the Stanford Synchrotron Radiation Lightsource, a national user facility operated by Stanford University on behalf of the U.S. Department of Energy, Office of Basic Energy Sciences. Software for analyzing GIWAXS data was written by Stefan Mannsfeld (SSRL), WxDiff code, and Joseph Kline (NIST) for an Igor analysis code.

REFERENCES AND NOTES

1 (a) Osaka, I.; Zhang, R.; Sauvé, G.; Smilgies, D.-M.; Kowalewski, T.; McCullough, R. D. *J. Am. Chem. Soc.* **2009,** *131*, 2521; (b) McCullough, I.; Heeney, M.; Bailey, C.; Genevicius, K.; Macdonald, I.; Shkunov, M.; Sparrowe, D.; Tierney, S.; Wagner, R.; Zhang, W.; Chabinyc, M. L.; Kline, R. J.; McGehee, M. D.; Toney, M. F. *Nat. Mater.* **2006,** *5*, 328; (c) Anthony, J. E. *Chem. Rev.* **2006,** *106*, 5028; (d) Ong, B. S.; Wu, Y.; Liu, P.; Gardner, S. *J. Am. Chem. Soc.* **2004,** *126*, 3378.

2 Zaumseil, J.; Sirringhaus, H. *Chem. Rev.* **2007,** *107*, 1296.

3 Babel, A.; Jenekhe, S. A. *J. Am. Chem. Soc.* **2003,** *125*, 13656.

4 (a) Chen, Z.; Zheng, Y.; Yan, H.; Facchetti, A. *J. Am. Chem. Soc.* **2009,** *131*, 8; (b) Jones, B. A.; Ahrens, M. J.; Yoon, M.-H.; Facchetti, A.; Marks, T. J.; Wasielewski, M. R. *Angew. Chem. Int. Ed.* **2004,** *43*, 6363.

5 Steckler, T. T.; Zhang, X.; Hwang, J.; Honeyager, R.; Ohira, S.; Zhang, X.-H.; Grant, A.; Ellinger, S.; Odom, S. A.; Sweat, D.; Tanner, D. B.; Rinzler, A. G.; Barlow, S.; Brédas, J.-L.; Kippelen, B.; Marder, S. R.; Reynolds, J. R. *J. Am. Chem. Soc.* **2009,** *131*, 2824.

6 Usta, H.; Facchetti, A.; Marks, T. J. *J. Am. Chem. Soc.* **2008,** *130*, 8580.

7 (a) Facchetti, A.; Yoon, M.-H.; Stern, C. L.; Hutchison, G. R.; Ratner, M. A.; Marks, T. J. *J. Am. Chem. Soc.* **2004,** *126*, 13480; (b) Yoon, M.-H.; DiBenedetto, S. A.; Facchetti, A.; Marks, T. J. *J. Am. Chem. Soc.* **2005,** *127*, 1348; (c) Ie, Y.; Nitani, M.; Ishikawa, M.; Nakayama, K.-i.; Tada, H.; Kaneda, T.; Aso, Y. *Org. Lett.* **2007,** *9*, 2115; (d) Ie, Y.; Umemoto, Y.; Okabe, M.; Kusunoki, T.; Nakayama, K.-i.; Pu, Y.-J.; Kido, J.; Tada, H.; Aso, Y. *Org. Lett.* **2008,** *10*, 833.

8 Dell, E. J.; Campos, L. M. *J. Mater. Chem.* **2012,** *22*, 12945.

9 (a) Barbarella, G.; Pudova, O.; Arbizzani, C.; Mastragostino, M.; Bongini, A. *J. Org. Chem.* **1998,** *63*, 1742; (b) Arbizzani, C.; Barbarella, G.; Bongini, A.; Favaretto, L.; Masragostino, M.; Ostoja, P.; Pudova, O.; Zambianchi, M. *Opt. Mater.* **1998,** *9*, 43; (c) Yamamoto, T.; Nurulla, I.; Hayashi, H.; Koinuma, H. *Synth. Metals* **1999,** *107*, 137; (d) Zhang, C.; Nquyen, T. H.; Sun, J.; Li, R.; Black, S.; Bonner, C. E.; Sun, S.-S. *Macromolecules* **2009,** *42*, 663; (e) King, S. M.; Perepichka, I. I.; Perepichka, I. F.; Dias, F. B.; Bryce, M. R.; Monkman, A. P. *Adv. Funct. Mater.* **2009,** *19*, 1.

10 (a) Vorontsova, L. G. *J. Struct. Chem.* **1966,** *7*, 234; (b) Miyahara, Y.; Inazu, T. *Tetrahedron Lett.* **1990,** *31*, 5955; (c) Rozen, S.; Bareket, Y. *J. Org. Chem.* **1997,** *62*, 1457.

11 Amir, E.; Rozen, S. *Angew. Chem. Int. Ed.* **2005,** *44*, 7374.

12 Amir, E.; Sivanandan, K.; Cochran, J. E.; Cowart, J. J.; S. Y. Ku, Seo, J. H.; Chabinyc, M. L.; Hawker, C. J. *J. Polym. Sci. Part A: Polym. Chem.* **2011,** *49*, 1933.

13 Wasserman, S. R.; Tao, Y. T.; Whitesides, G. M. *Langmuir* **1989,** *5*, 1074.

14 Factor, B. J.; Russell, T. P.; Toney, M. F. *Macromolecules* **1993,** *26*, 2847.

15 Mannsfeld, S. C. B.; Tang, M. L.; Bao, Z. *Adv. Mater.* **2011,** *23*, 127.

16 Horowitz, G. *Adv. Mater.* **1998,** *10*, 365.

17 Brédas, J.-L., Cornil, J.; Heeger, A. J. *Adv. Mater.* **1996,** *8*, 447.

18 Kim, M. G.; Lee, H. G.; Kim, B. H.; Kim, J. S.; Park, Y. W. *Phys. Scripta* **2005,** *T115*, 393.

19 Kim, B. G.; Chung, J. S.; Sohn, E. S.; Kwak, S. Y.; Lee, J. C. *Macromolecules* **2009,** *42*, 3333–3339.

20 Yates, B. W.; Shinozaki, D. M.; Kumar, A.; Meath, W. J. *J. Polym. Sci. Part B: Polym. Phys.* **1993,** *31*, 1837–1844.

21 Pangher, N.; Wilde, L.; Polcik, M.; Haase, J. *Surf. Sci.* **1997,** *332*, 211–222.

22 (a) Ljungqvist, N.; Hjertberg, T. *Macromolecules* **1995,** *28*, 5993–5999; (b) Manceau, M.; Rivaton, A.; Gardette, J.; Guillerez, S.; Lemaitre, N. *Polym. Degrad. Stabil.* **2009,** *94*, 898–907.

23 Louarn, G.; Buisson, J. P.; Lefrant, S.; Fichou, D. *J. Phys. Chem.* **1995,** *99*, 11399.

24 Sirringhaus, H.; Brown, P. J.; Friend, R. H.; Nielsen, M. M.; Bechgaard, K.; Langeveld-Voss, B. M. W.; Splering, A. J. H.; Janssen, R. A. J.; Meljer, E. W.; Herwig, P.; de Leeuw, D. M. *Nature* **1999,** *401*, 685.

25 Gallazzi, M. C.; Castellani, L.; Marin, R. A.; Zerbi, G. *J. Polym. Sci. Part A: Polym. Chem.* **1993,** *31*, 3339.

26 Wu, Y.; Liu, P.; Gardner, S.; Ong, B. S. *Chem. Mater.* **2005,** *17*, 221.

27 Anthony, J. E.; Eaton, D. L.; Parkin, S. R. *Org. Lett.* **2002,** *4*, 15.

28 Kline, R. J.; Chabinyc, M. L.; Toney, M. F.; McCulloch, I.; Heeney, M. *J. Am. Chem. Soc.* **2007,** *129*, 3226.

29 Cramer, C. J. Essentials of Computational Chemistry; John Wiley & Sons: New York, **2004.**

30 DeLongchamp, D. M.; Kline, R. J.; Jung, J.; Lin, E. K.; Fischer, D. A.; Gundlach, D. J.; Cotts, S. K.; Moad, A. J.; Richter, L. J.; Toney, M. F. *Macromolecules* **2008,** *41*, 5709.

31 Bredas, J. L.; Calbert, J. P.; *Proc. Natl. Acad. Sci. USA* **2002,** *99*, 5804.

32 Jimison, L. H.; Salleo, A.; Chabinyc, M. L.; Bernstein, D. P.; Toney, M. F. *Phys. Rev. B* **2008,** *78*, 125319.

33 Ling, M. M.; Bao, Z. *Chem. Mater.* **2004,** *16*, 4824.

34 (a) Anthony, J. E.; Heeney, M.; Ong, B. S. *MRS Bull.* **2008,** *33*, 698–705; (b) Salleo, A.; Chabinyc, M. L. Organic Electronics: Materials, Manufacturing and Applications; Wiley-VCH Verlag GmbH & Co. KGaA: Weinheim, **2006;** Chapter 5.